Environmental Science & Technology

Article

pubs.acs.org/est

Quantitative Identification of Metastable Magnesium Carbonate Minerals by Solid-State ^{13}C NMR Spectroscopy

Jeremy K. Moore,[†] J. Andrew Surface,[†] Allison Brenner,[†] Philip Skemer,[§] Mark S. Conradi,[‡,†] and Sophia E. Hayes*[,†]

[†]Department of Chemistry, Washington University, One Brookings Drive, Saint Louis, Missouri, 63130, United States

[‡]Department of Physics, Washington University, One Brookings Drive, Saint Louis, Missouri, 63130, United States

[§]Department of Earth and Planetary Sciences, Washington University, One Brookings Drive, Saint Louis, Missouri, 63130, United States

Supporting Information

ABSTRACT: In the conversion of CO_2 to mineral carbonates for the permanent geosequestration of CO_2, there are multiple magnesium carbonate phases that are potential reaction products. Solid-state ^{13}C NMR is demonstrated as an effective tool for distinguishing magnesium carbonate phases and quantitatively characterizing magnesium carbonate mixtures. Several of these mineral phases include magnesite, hydromagnesite, dypingite, and nesquehonite, which differ in composition by the number of waters of hydration or the number of crystallographic hydroxyl groups. These carbonates often form in mixtures with nearly overlapping ^{13}C NMR resonances which makes their identification and analysis difficult. In this study, these phases have been investigated with solid-state ^{13}C NMR spectroscopy, including both static and magic-angle spinning (MAS) experiments. Static spectra yield chemical shift anisotropy (CSA) lineshapes that are indicative of the site-symmetry variations of the carbon environments. MAS spectra yield isotropic chemical shifts for each crystallographically inequivalent carbon and spin−lattice relaxation times, T_1, yield characteristic information that assist in species discrimination. These detailed parameters, and the combination of static and MAS analyses, can aid investigations of mixed carbonates by ^{13}C NMR.

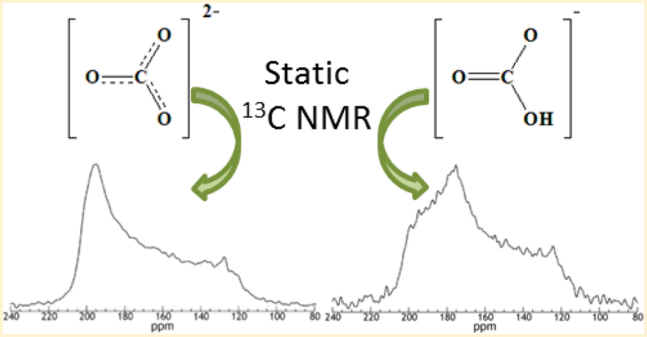

INTRODUCTION

Many CO_2 capture and sequestration studies have focused on the formation of magnesium carbonate minerals from mafic and ultramafic protoliths as a permanent storage solution for CO_2. These reaction products are often imprecisely described as magnesite ($MgCO_3$), the energetically favored magnesium carbonate. There are, however, additional thermodynamically metastable phases that include waters of crystallization and hydroxyl groups in the crystal structure.[1,2] These metastable minerals form due to kinetic trapping along the reaction pathway to magnesite. The lifetime of the metastable magnesium carbonate minerals can be long, even relative to geologic time scales, since the energy needed to remove a water from the crystal structure is not always available to the system.[1] There are many possible forms of these hydroxy-hydrated magnesium carbonates: some examples, listed from least hydrated to most, include hydromagnesite [$4MgCO_3{\cdot}Mg(OH)_2{\cdot}4H_2O$], dypingite [$4MgCO_3{\cdot}Mg(OH)_2{\cdot}(5-8)H_2O$], and nesquehonite [$Mg(OH)(HCO_3){\cdot}2H_2O$].

In CO_2 sequestration reactions, it has been reported that Mg-containing minerals react with CO_2 to form products consisting of a mixture of hydroxy-hydrated magnesium carbonates and magnesite.[1,3−7] The specific composition of these product mixtures is dependent on the reactant minerals and reaction conditions, such as temperature and pH.[1,8−11]

The ability to distinguish and quantify the product minerals in a mixture of magnesium carbonate phases is difficult due to a combination of factors. One complicating factor is that reaction products often form mixtures of amorphous and crystalline species,[12−14] and current methods such as powder X-ray diffraction (pXRD) cannot identify the amorphous components. Additionally, multiple possible hydrated magnesium carbonates can be produced as well as adducts that form with ions, such as Na^+ and Ca^{2+}. Here we will demonstrate the ability of NMR to identify these mineral phases and quantitatively characterize these species in mixtures, thereby facilitating the study of sequestration reactions and their kinetics.

Received: July 14, 2014
Revised: October 28, 2014
Accepted: December 1, 2014

   dx.doi.org/10.1021/es503390d | Environ. Sci. Technol. XXXX, XXX, XXX−XXX

Solid-state nuclear magnetic resonance (NMR) spectroscopy is a powerful tool for identification of various carbonate species,[2,14−19] despite having relatively small structural differences between them. Pure $MgCO_3$ phases are needed as standards for rigorous NMR characterization, and we present synthesis methods to obtain these for each of the metastable minerals. The NMR signatures of magnesite, hydromagnesite, dypingite, and nesquehonite are established through a suite of ^{13}C NMR techniques from the pure mineral samples, with assignments confirmed by Raman spectroscopy and pXRD.

NMR measurements used for this work include $^{13}C\{^1H\}$ magic angle spinning (MAS) NMR with proton decoupling (denoted by ^1H in brackets) and $^{13}C\{^1H\}$ cross-polarization magic angle spinning (CPMAS) NMR. When employed, MAS NMR narrows resonances that are broadened by dipolar coupling, as well as chemical shift anisotropy (CSA). As a result, narrow resonances are observed at a species' isotropic chemical shift (δ^{iso}). MAS NMR allows the minerals to be distinguished by both the chemical shift and the number of peaks which corresponds to the number of crystallographically inequivalent ^{13}C sites. Static ^{13}C NMR yields a characteristic line shape from broadening of the NMR resonance through the CSA. These broad "powder patterns" can be used to distinguish the symmetry of the chemical environment of the ^{13}C in the product mineral.[15,20−23] Static ^{13}C NMR resonances are defined by components evident in the CSA line shape—namely, their isotropic chemical shift (δ^{iso}), chemical shift anisotropy (δ^{aniso}), and asymmetry (η). These parameters are determined by the shape of the static NMR CSA powder pattern and are unique for each metastable magnesium carbonate mineral based on the carbon atoms' nearby environments.

With this detailed characterization, it is possible to distinguish these products in a variety of settings, including analysis from in situ and ex situ NMR experiments.[2,19] The ^{13}C MAS NMR, pXRD, and Raman spectroscopy each lend themselves to ex situ characterization of subsets of the product minerals which allow, for example, the study of compositional gradients within a reactor. The ^{13}C static NMR gives the capability for in situ monitoring of the mineral and CO_2 reaction ensemble that forms these mixtures of metastable magnesium carbonates. Using the magnesium carbonate phases and the quantitative characterization afforded by solid-state NMR, the capability of distinguishing and quantifying kinetically trapped magnesium carbonate minerals is possible in both in situ and ex situ NMR experiments.

MATERIALS AND METHODS

Magnesite, $MgCO_3$, was synthesized in a high temperature, elevated pressure vessel for use in analyzing the reaction in situ with ^{13}C static NMR as described previously.[2] Samples were prepared by adding 1.60 g of forsterite, Mg_2SiO_4, powder and 2.77 mL deionized (DI) water into the reaction vessel. The vessel was then pressurized with 110 atm of $^{13}CO_2$ generated through cryogenic pressure intensification and then heated to 90 °C. The mixture was then allowed to react for 8 days. Magnesite is the thermodynamically favored product from reactions with forsterite at these elevated temperatures and pressures, and therefore was formed preferentially.[1,3,24−27] The magnesite precipitates on the surface of the forsterite particles.

Hydromagnesite, $[4MgCO_3{\cdot}Mg(OH)_2{\cdot}4H_2O]$, was synthesized[28,29] by adding 0.107 g of 99% ^{13}C enriched $NaHCO_3$ to a solution of 0.245 g of $MgCl_2$ in 8.0 mL of DI water. The solution was mixed for 1 min, and then allowed to react for 4 days at 92 °C. The precipitate was filtered and dried under vacuum for 24 h at room temperature.

Dypingite, $[4MgCO_3{\cdot}Mg(OH)_2{\cdot}(5{-}8)H_2O]$, was synthesized[7,28,29] by adding 0.221 g of 99% ^{13}C enriched $NaHCO_3$ to a solution of 0.251 g of $MgCl_2$ in 3.25 mL of DI water. This solution reacted for 24 h at room temperature, followed by 48 h of reaction at 62 °C, finally reacting for 24 h at 72 °C. The precipitate was then filtered and dried under vacuum for 24 h at room temperature.

Nesquehonite, $[Mg(OH)(HCO_3){\cdot}2H_2O]$, was synthesized[28−30] by adding 0.146 g of 99% ^{13}C enriched $NaHCO_3$ to a solution of 0.164 g of $MgCl_2$ in 3.25 mL of deionized (DI) water.[30] The solution was stirred for 1 min, and the glass beaker was sealed. The solution reacted for 3 days at room temperature. The precipitate was collected by filtering the sample, drying under vacuum at 40 °C for 10 min, followed by air drying overnight. The powder was then rinsed with DI water before repeating the filtering and drying procedure. The mineral assignments were confirmed by pXRD and ^{13}C NMR.

The NMR measurements were acquired on a 7 T magnet with a ^1H frequency of 299.673 MHz and a ^{13}C frequency of 75.365 MHz with a commercial HX MAS Chemagnetics probe. $^{13}C\{^1H\}$ MAS and static NMR spectra were acquired in a single scan by a Bloch decay sequence with decoupling during acquisition (28.4 kHz typical decoupling strengths) spinning frequency (ν_R, MAS only) of 5 kHz, using a $\pi/2$ pulse length of 8.8 μs, and allowing the sample to reach thermal equilibrium in the magnetic field over 45 min. $^{13}C\{^1H\}$ CPMAS cross-polarization "build-up" curves and spectra were acquired with ν_R of 5 kHz, a recycle delay of 5 s, and recording 32 transients. The B_1 field strengths were 27.8 kHz which gave a ^1H $\pi/2$ pulse length of 9 μs. The matching condition for the contact period was found by the Hartmann−Hahn match and the B_1 fields were not modulated during the contact time. Typical cross-polarization contact times (τ_{cp}) of 100 μs to 15 ms were used to obtain the "build-up" curves. Chemical shifts were referenced to adamantane at 29.45 ppm. The isotropic chemical shifts for the static spectra were assigned via peak fitting and confirmed with slow spinning MAS NMR. Some samples were comixed with a carbon-free powder, forsterite, due to limited sample quantity (for the purpose of filling a NMR rotor volume).

The relaxation time T_1 was measured by $^{13}C\{^1H\}$ MAS NMR saturation recovery pulse sequence and fitting the peak area versus delay time curve. The $T_{1\rho}$ and T_{IS} were measured with $^{13}C\{^1H\}$ CPMAS NMR and fitting the cross-polarization "build-up" curve. The peak areas were collected from the fits of the data.

All NMR spectra were fit with DMFIT.[31] δ^{iso} is the isotropic chemical shift and is defined as $1/3(\delta_{XX}+\delta_{YY}+\delta_{ZZ})$. The principal values of the CSA powder pattern are defined as $|\delta_{ZZ}-\delta^{iso}|>|\delta_{XX}-\delta^{iso}|>|\delta_{YY}-\delta^{iso}|$. The anisotropic chemical shift is defined as $\delta^{aniso} = \delta_{ZZ}-\delta^{iso}$. Finally, the asymmetry is defined as $\eta = (\delta_{YY}-\delta_{XX})/\delta^{aniso}$.

The Raman spectra were acquired on a HoloLab Series 5000 Laser Raman Microprobe with a 532 nm laser beam at 11 mW of power. The resolution was approximately 3 cm^{-1}, and sampled regions were approximately 5 μm in diameter. The reproducibility of the Raman data were better than 1 cm^{-1}.

The pXRD data were obtained on a Rigaku Geigerflex D-MAX/A diffractometer with Cu−Kα radiation at 35 kV and 35 mA. Values of 2θ ranged from 6° to 60° with a step size of

dx.doi.org/10.1021/es503390d | Environ. Sci. Technol. XXXX, XXX, XXX−XXX

Table 1. Summary of NMR Parameters and Relaxation Time Constants

	minerals						
	magnesite	hydromagnesite			dypingite		nesquehonite
^{13}C δ^{iso} (ppm)	169.9	165.2	163.1	162.5	165.3	163.5	165.4
% area for each C site	100	51.8	48.4		60.7	39.3	100
^{13}C δ_{xx} (ppm)	204.2	193.9	203.9		193.0	205.8	204.1
^{13}C δ_{yy} (ppm)	196.8	186.4	175.0		184.9	175.1	178.1
^{13}C δ_{zz} (ppm)	118.8	115.8	110.5		118.0	109.6	115.1
^{13}C η	0.14	0.16	0.55		0.17	0.57	0.51
^{13}C δ^{aniso} (ppm)	−54.5	−47.4	−49.1		−47.3	−53.9	−50.6
^{13}C T_1 (s)	78.0	157	156		104	107	35.7
^{1}H $T_{1\rho}$ (ms)		7.1	3.5	8.0	4.8	3.7	58
T_{1S} (ms)		0.59	0.75	0.38	0.49	0.60	1.1

0.04° and 1 s intervals. Samples were held in a standard pXRD slide. Samples that had been comixed with forsterite, for the NMR studies, have peaks for this mineral in the pXRD patterns (as seen in Supporting Information (SI) Figures S2 and S3).

RESULTS AND DISCUSSION

The NMR spectrum of each mineral, both static and MAS, will be discussed individually, while the nuclear relaxation data will be discussed at the end, as to easily compare the minerals. All the relaxation data and CSA parameters are summarized in Table 1 and the CSA parameters are defined in the Materials and Methods section. The assignment of MAS NMR peaks was confirmed by slow spinning MAS NMR, which is discussed in the SI and shown in Figure S1. Schematics of the carbon sites present in the metastable magnesium carbonates are shown in Scheme 1. Shown are an axially symmetric CO_3^{2-} carbonate

Scheme 1. Schematic of Carbon Site Symmetry for CO_3^{2-} (Left) and HCO_3^- (Right)

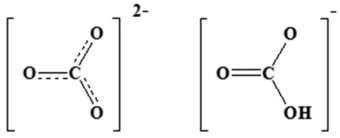

(D_{3h} point group) and a lower symmetry HCO_3^- bicarbonate species. Distinguishing between CO_3^{2-} and HCO_3^- is possible via their ^{13}C δ^{iso} chemical shifts, which have shifts of 170 and 160 ppm, respectively, in solution. Alternatively, the CSA line shape can be unambiguous for characterization in static ^{13}C NMR.

Magnesite. Magnesite, $MgCO_3$, precipitates during sequestration reactions on the surface of forsterite, the reactant mineral phase.[32,33] It forms directly in solutions with Mg^{2+} and CO_3^{2-} ions at temperatures above 120 °C but will form via an intermediate, hydromagnesite (that will be discussed later), even when the temperature is under 120 °C if given sufficient time. Magnesite is the only nonhydrated magnesium carbonate and has a single ^{13}C NMR resonance at 169.9 ppm as seen in static $^{13}C\{^1H\}$ NMR (Figure 1A) and $^{13}C\{^1H\}$ MAS NMR (Figure 1C, 1D).

The static spectrum has an asymmetry (η) of 0.14 and has a δ^{aniso} of −54.5 ppm. The asymmetry of pure crystalline magnesite is predicted to be 0, by the D_{3h} crystal symmetry of the ^{13}C carbonate site (as seen in Scheme 1), suggesting that sites within magnesite have disorder from the surfaces or grain boundaries between the magnesite particles and forsterite

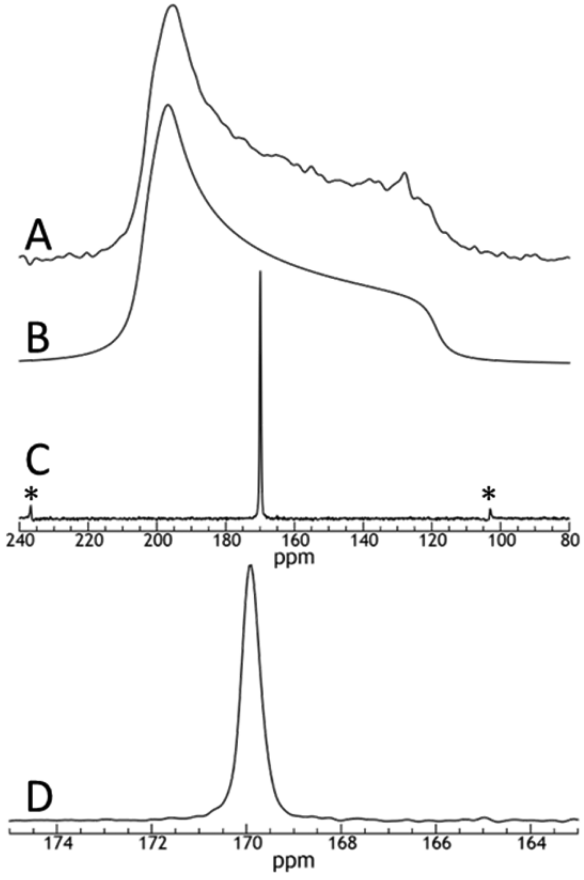

Figure 1. ^{13}C NMR of a magnesite ($MgCO_3$) mineral species grown on the surface of forsterite (Mg_2SiO_4). (A) Static $^{13}C\{^1H\}$ NMR. (B) Fit of the static ^{13}C NMR with parameters listed in Table 1. (C) $^{13}C\{^1H\}$ MAS NMR with ν_R = 5 kHz. (D) Expanded view of $^{13}C\{^1H\}$ MAS NMR. * denotes spinning sideband.

particles which cause deviations from pure $MgCO_3$. It has been reported previously that calcite ($CaCO_3$) can precipitate with protons in the crystal,[14,20] which could also account for a nonzero asymmetry of the powder pattern. Further evidence of protons in magnesite's crystal structure can be seen in a separate reaction that ran for a shorter time as seen in Figure 2, where the magnesite peak appears with a shoulder.

This pair of resonances, seen in Figure 2, represents a magnesite phase with nearby protons and a proton-free magnesite phase. Both samples from Figure 1and Figure 2 appear as magnesite alone in pXRD and Raman spectroscopy

dx.doi.org/10.1021/es503390d | Environ. Sci. Technol. XXXX, XXX, XXX−XXX

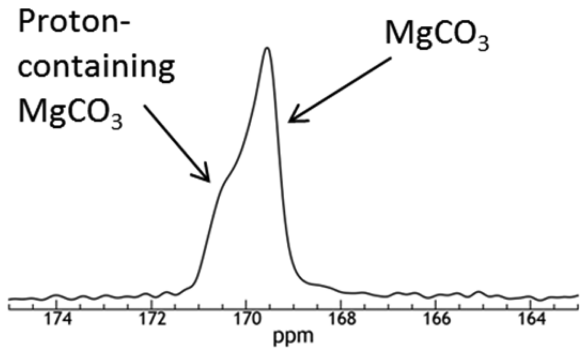

Figure 2. $^{13}C\{^1H\}$ MAS NMR of a mineral containing magnesite and magnesite with nearby protons with ν_R = 5 kHz.

(seen in SI Figure S2). It is also possible to cross-polarize the proton-containing magnesite peak with CPMAS proving that there are indeed protons nearby the magnesite carbon (CO_3^{2-}) in the higher frequency peak. The shift to higher frequency was reported in a hydrated calcium carbonate.[14] Other evidence used in assigning the higher frequency peak to the proton-containing magnesite species is comparing the peak fwhm. The fwhm of the peak in Figure 1 is 0.46 ppm. The peak at 169.5 ppm in Figure 2 has a fwhm of 0.57 ppm while the fwhm of the peak at 170.2 ppm is 1.08 ppm. Since the low frequency peak in Figure 2 and the peak in Figure 1 have a similar fwhm, the structures have similar crystallinity which can be dictated by the presence of protons. The high frequency peak in Figure 2, however, is broadened, presumably by nearby protons.

Hydromagnesite. Hydromagnesite forms in sequestration reactions as a mixture with dypingite, described below, in solutions with high concentrations of Mg^{2+}, HCO_3^-, and CO_3^{2-} and temperatures between 40 and 120 °C.[1,6,28] However, hydromagnesite can be synthesized in isolated form in benchtop reactions. There are two crystallographically inequivalent carbons in the crystal structure of hydromagnesite,[34−36] seen in the ^{13}C NMR spectra of Figure 3, and the assignment has been confirmed with pXRD (SI Figure S3). Hydromagnesite is the least hydrated metastable magnesium carbonate, the H_2O/Mg ratio being 0.8, the composition of hydromagnesite being $[4MgCO_3{\cdot}Mg(OH)_2{\cdot}4H_2O]$.

The two resonances have isotropic ^{13}C chemical shifts of 165.2 and 163.0 ppm. These peaks, respectively, account for 51.8% and 48.2% of the integrated area signifying that the two sites are approximately equally populated in the mineral, as expected. The asymmetry of the CSA line shape shows one peak (δ_{iso} = 165.2 ppm) as nearly axially symmetric and the other (δ_{iso} = 163.0 ppm) as more asymmetric with η values of 0.16 and 0.55 respectively. These CSA parameters indicate that one of the carbon sites in the crystal structure is similar to that of magnesite, which is axially symmetric, while the other site has an asymmetry similar to the asymmetric nesquehonite carbon, as will be seen below.

When using CPMAS NMR, the resonance at 163.0 ppm split into two resonances (as seen in SI Figure S4) with different values for the time constants $T_{1\rho}$ and T_{IS} for each resonance. This split resonance reveals why the peak at 163.0 ppm is shorter and broader than the peak at 165.2 ppm: the peak at lower frequency appears to be made up of at least two resonances. These data indicate the nesquehonite-like carbon, 163.0 ppm, has more disorder caused by multiple configurations, likely due to nearby waters of crystallization.

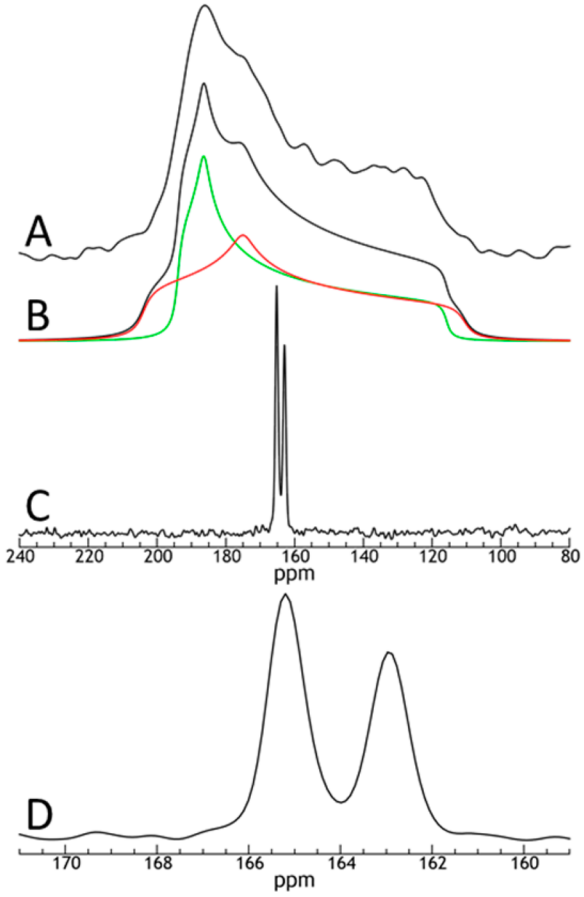

Figure 3. ^{13}C NMR of a hydromagnesite, $[4MgCO_3{\cdot}Mg(OH)_2{\cdot}4H_2O]$, mineral. (A) Static $^{13}C\{^1H\}$ NMR. (B) Fit of the static ^{13}C NMR with the overall fit in black and the individual sites fitted in red and green and parameters listed in Table 1. (C) $^{13}C\{^1H\}$ MAS NMR with ν_R = 5 kHz. The peak at 165.2 ppm is the green powder pattern and the peak at 163.0 ppm is the red powder pattern. (D) Expanded view of $^{13}C\{^1H\}$ MAS NMR.

Dypingite. Dypingite forms in sequestration reactions as a mixture with hydromagnesite in solutions with high concentrations of Mg^{2+}, HCO_3^-, and CO_3^{2-} and temperatures between 40 and 120 °C.[7,10,37,38] Here we were able to isolate a nearly pure dypingite mineral. There is no known crystal structure for dypingite, but the mineral has a unique pXRD pattern (SI Figure S5).[7,38−40] The current convention is that dypingite is any hydroxy-hydrated magnesium carbonate with 5 to 8 waters of hydration[7,11] and the formula $[4MgCO_3{\cdot}Mg(OH)_2{\cdot}xH_2O]$, (where x = 5−8) giving a H_2O/Mg ratio of 1−1.6. This makes a pure phase difficult to synthesize; nevertheless, this mineral still has distinguishable NMR features.[19] Figure 4 shows the static and MAS $^{13}C\{^1H\}$ NMR of the dypingite sample.

Two NMR resonances are apparent in the ^{13}C MAS NMR spectrum (see Figure 4C and 4D) with isotropic chemical shifts of 165.3−163.5 ppm, and each has a unique CSA line shape. There is a small impurity resonance (Figure 4D) at 166.5 ppm (which notably does not match the δ_{iso} chemical shift of any other species we've observed so far). These resonances indicate the presence of two crystallographically inequivalent carbons. The difference is apparent in the asymmetry of the powder patterns, where the peak at δ^{iso} = 165.3 ppm is magnesite-like with an η value of 0.17 and a δ^{aniso} value of −47.3 ppm, while

dx.doi.org/10.1021/es503390d | Environ. Sci. Technol. XXXX, XXX, XXX−XXX

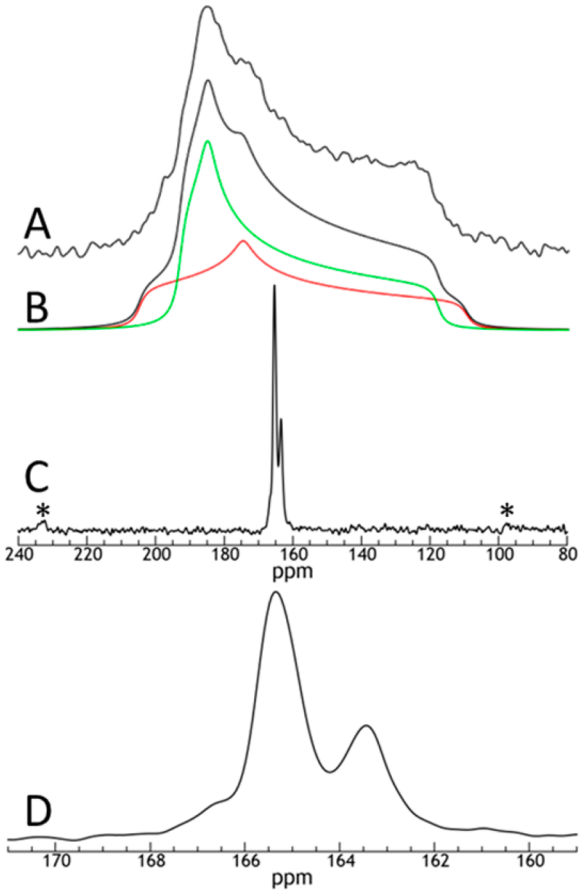

Figure 4. ^{13}C NMR of a nearly pure dypingite, $[4MgCO_3{\cdot}Mg(OH)_2{\cdot}(5{-}8)H_2O]$, mineral. (A) Static $^{13}C\{^1H\}$ NMR. (B) Fit of the static ^{13}C NMR with the overall fit in black and the individual sites fitted in red and green and parameters listed in Table 1. (C) $^{13}C\{^1H\}$ MAS NMR with ν_R = 5 kHz. The peak at 165.3 ppm is the green powder pattern and the peak at 163.5 ppm is the red powder pattern. (D) Expanded view of $^{13}C\{^1H\}$ MAS NMR. * denotes spinning sideband.

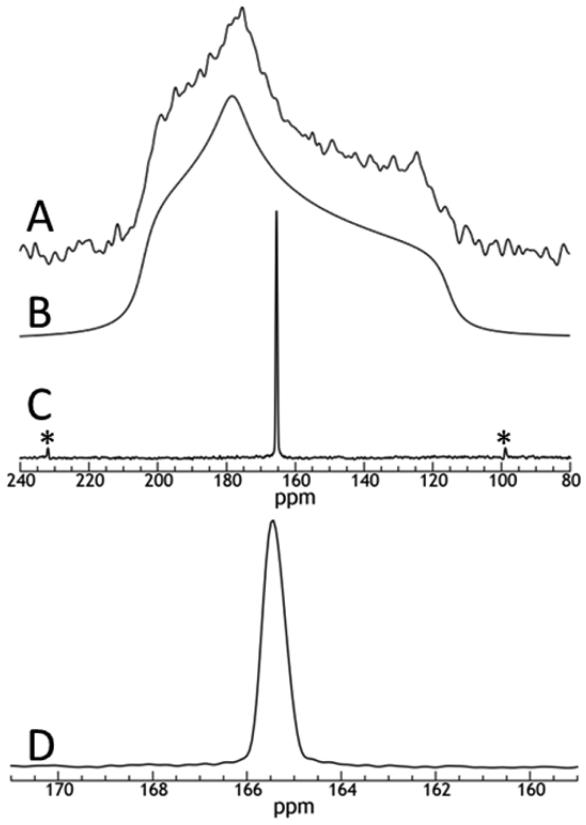

Figure 5. ^{13}C NMR of a nesquehonite mineral. (A) Static $^{13}C\{^1H\}$ NMR. (B) Fit of the static ^{13}C NMR with parameters listed in Table 1. (C) $^{13}C\{^1H\}$ MAS NMR with ν_R = 5 kHz. (D) Expanded view of $^{13}C\{^1H\}$ MAS NMR. * denotes spinning sideband.

the peak at δ^{iso} = 163.5 ppm is more asymmetric with an η value of 0.57 and a δ^{aniso} value of −53.9 ppm. Even without a known crystal structure, the appearance of two crystallographically inequivalent carbon sites in dypingite is encouraging because the composition only differs from hydromagnesite (with two unique carbons) by the number of waters of hydration. The resonance at 165.3 ppm comprises 60.7% of the integrated area of the spectrum, meaning that approximately 3 out of every 5 carbon sites are in the magnesite-like electronic environment. To identify dypingite with ^{13}C NMR it is important to check the area ratio of the peaks since this area ratio of 3:2 for the resonances at 165.3 and 163.5 ppm is different from that of hydromagnesite (with its 1:1 ratio for the two sites), since the two chemical shift values are very close.

Nesquehonite. The mineral nesquehonite is the most hydrated magnesium carbonate phase included here, with a H_2O/Mg ratio of 2, and has a chemical composition of $[Mg(OH)(HCO_3){\cdot}2H_2O]$.[41] This species has also been described as $[MgCO_3{\cdot}3H_2O]$,[30,42,43] which will be discussed more below. This hydroxy-hydrated magnesium carbonate is the preferential product in systems with high concentrations of Mg^{2+}, HCO_3^-, and CO_3^{2-} and temperatures below 40 °C.[28,30,44,45] The crystal structure of nesquehonite contains only one crystallographically inequivalent carbon.[43,46] Therefore, only one NMR resonance is expected, and this resonance can be distinguished in both the static (Figure 5A) and MAS $^{13}C\{^1H\}$ NMR (Figure 5C, and D) spectra and is confirmed by pXRD and Raman in SI Figure S6.

The isotropic chemical shift, which can be seen in Figure 5C and 5D, is 165.4 ppm. The fit of the static spectrum gives an asymmetry (η) of 0.51, a symmetry close to that of the bicarbonate structure seen in Scheme 1, and an anisotropic shift (δ^{aniso}) of −50.64 ppm. We note that some previous studies report that nesquehonite has two ^{13}C resonances,[26,47] but the crystal structure from X-ray diffraction dictates otherwise. From further studies (as seen in SI Figure S7), we conclude that this second resonance is a northupite impurity in nesquehonite, arising from incomplete sample purification and the presence of excess Na^+ from the synthesis. This assignment is confirmed by pXRD (SI Figure S8B−E), Raman (SI Figure S8A), and $^{23}Na\{^1H\}$ MAS NMR (SI Figure S9).

The large degree of asymmetry of the static line shape suggests that the symmetry of the ^{13}C site is far from that of D_{3h} (see Scheme 1). The chemical shift is at a lower frequency than magnesite suggesting that the complex $[Mg(OH)(HCO_3){\cdot}2H_2O]$ (as opposed to $MgCO_3{\cdot}3H_2O$) is the more accurate description due to its variation from the carbonate-like environment. Confirming evidence based on the relaxation times is discussed below.

Comparison of Minerals and Techniques. Nuclear spin relaxation times (^{13}C T_1, ^1H $T_{1\rho}$, and T_{IS}) can be used to determine the carbon atom environment and the dynamics of nearby protons in the mineral species. A summary of the

dx.doi.org/10.1021/es503390d | Environ. Sci. Technol. XXXX, XXX, XXX−XXX

nuclear spin time constants is presented in Table 1 in addition to the principal values of the ^{13}C CSA tensor and CSA parameters previously discussed. The isotropic chemical shifts were determined from the $^{13}C\{^1H\}$ MAS NMR spectra.

The ^{13}C T_1 (spin−lattice) relaxation times across all four minerals reveal a trend that may prove predictive for other mineral phases. The T_1 time increases from nesquehonite to dypingite to hydromagnesite. This trend indicates that the more hydrated the mineral phase, the faster the T_1 relaxation, due to coupling with the H_2O in the crystal structure. The T_1 for magnesite is shorter than the hydroxy-hydrated carbonates despite the expectation of a longer T_1 relaxation time in this nonhydrated mineral. Possible explanations are that paramagnetic impurities dominate the T_1 relaxation in magnesite or that the proximity of the ^{13}C enriched carbonates in magnesite will enhance the effects of the homonuclear dipole−dipole spin−lattice relaxation mechanism.[48] (Note: the homonuclear dipole−dipole T_1 mechanism is not present in natural abundance magnesite and therefore, is expected to have a longer T_1.) The relaxation time trend is important information when studying new mineral phases since the T_1 analysis ensures quantitative characterization in both in situ and ex situ CO_2 mineralization reactions and is informative of the level of hydration of the mineral phase.

The ^1H $T_{1\rho}$ relaxation time is in the rotating frame, and T_{IS} is the CP-buildup time governed by $^{13}C-^1H$ dipolar coupling. In nesquehonite, the relatively long $T_{1\rho}$ time constant could indicate that the protons near the carbon in this mineral have little motion. As stated before, this structure has been published as both $[MgCO_3{\cdot}3H_2O]$ and $[Mg(OH)(HCO_3){\cdot}2H_2O]$. For the nearest proton to be relatively static, the latter of these, the magnesium bicarbonate structure, is the one most consistent with the $T_{1\rho}$ data (and is consistent with the ^{13}C line shape shown in Figure 5A). The shorter $T_{1\rho}$ in dypingite and hydromagnesite, may reflect nearby proton dynamics from the waters of crystallization; however, it is also possible that the purity and crystallinity of the sample could lead to the shorter $T_{1\rho}$.

We are able to see two types of carbon symmetries in these minerals based on the values of η. Asymmetry values close to 0.5 are structures that resemble the bicarbonate-like carbon environment, while values close to 0.1 are structures close to the D_{3h} magnesite carbon environment (both seen in Scheme 1). Static NMR CSA powder patterns are therefore seen to be helpful in determining local carbon structure.

Dypingite and hydromagnesite have very similar structures seen in the chemical shift and asymmetry. One key differentiating factor is the relative fraction of carbons in each type of structure. Dypingite has a 3:2 ratio of carbons, with three of the carbon sites having an η value close to 0.1 and two carbon sites with an η value close to 0.5. However, hydromagnesite has a 1:1 ratio of these two sites. Another difference is seen in the T_1 relaxation times: the hydromagnesite T_1 relaxation is longer by approximately 50 s. By measuring the T_1 relaxation time and the area of the two peaks, dypingite and hydromagnesite are able to be distinguished. These differences will aid in quantifying a mixture of these products since a mixture will exhibit a weighted average of these values. Knowing the relaxation times and integrated areas for each mineral species allows quantification of dypingite and hydromagnesite individually from a mixture.

The information on each of these minerals is relevant to future NMR studies, both in situ and ex situ. The in situ NMR technique gives the full complement of the reacting system while ex situ analysis has the ability to characterize subsets of the reaction mixture.

In situ NMR measurements are of significant interest because these reactions can be completed in a reactor that mimics CO_2 sequestration processes.[2] In situ NMR provides a spectroscopic "window" into the product mineral formation, which is important because the pH, reactant minerals, and temperature all affect the product outcome. Such techniques have been used to observe the speciation of ^{13}C as it is introduced from enriched $^{13}CO_2$ gas under geologic sequestration conditions (i.e., ∼80 °C, ∼80 atm).[2] These experiments benefit from methods that allow a high pressure of CO_2 to remain on the reacting system which forces the CO_2 to remain in solution and thus accessible for reaction. This high pressure reaction environment is easily achievable with static ^{13}C NMR, therefore this technique can monitor the reaction continuously.

Ex situ NMR measurements involve collecting the reacted mineral sample and running $^{13}C\{^1H\}$ MAS (or CPMAS) NMR experiments on the product. The reaction products are then distinguished by their crystallographically inequivalent ^{13}C sites, which are each indicated by an individual ^{13}C chemical shift. This technique can therefore be used to characterize spatial product gradients that form during the sequestration reactions, by sectioning the product as a function of depth in a fixed bed reactor or sample chamber. When *in situ* and *ex situ* ^{13}C NMR techniques are used together, the combined information can be integrated to give a full picture of the reaction and its associated products.

■ ASSOCIATED CONTENT

Supporting Information

Included are Raman spectra, powder X-ray diffraction (pXRD) patterns, $^{13}C\{^1H\}$ MAS at slow spinning speeds, and $^{23}Na\{^1H\}$ magic angle spinning (MAS) NMR spectra that confirm the NMR assignments in this article. This material is available free of charge via the Internet at http://pubs.acs.org.

■ AUTHOR INFORMATION

Corresponding Author

*Phone: (314) 935-4624; fax: (314) 935-4481; e-mail: hayes@wustl.edu.

Notes

The authors declare no competing financial interest.

■ ACKNOWLEDGMENTS

We thank the Washington University in St. Louis, Consortium for Clean Coal Utilization (CCCU) for funding.

■ REFERENCES

(1) Hänchen, M.; Prigiobbe, V.; Baciocchi, R.; Mazzotti, M. Precipitation in the Mg-carbonate system — effects of temperature and CO_2 pressure. *Chem. Eng. Sci.* **2008**, *63*, 1012−1028.

(2) Surface, J. A.; Skemer, P.; Hayes, S. E.; Conradi, M. S. In situ measurement of magnesium carbonate formation from CO_2 using static high-pressure and -temperature ^{13}C NMR. *Environ. Sci. Technol.* **2013**, *47*, 119−125.

(3) Bénézeth, P.; Saldi, G. D.; Dandurand, J.-L.; Schott, J. Experimental determination of the solubility product of magnesite at 50 to 200°C. *Chem. Geol.* **2011**, *286*, 21−31.

(4) Zhao, L.; Sang, L.; Chen, J.; Ji, J.; Teng, H. H. Aqueous carbonation of natural brucite: Relevance to CO_2 sequestration. *Environ. Sci. Technol.* **2010**, *44*, 406−411.

(5) King, H. E.; Plümper, O.; Putnis, A. Effect of secondary phase formation on the carbonation of olivine. *Environ. Sci. Technol.* **2010**, *44*, 6503−6509.
(6) Case, D. H.; Wang, F.; Giammar, D. E. Precipitation of magnesium carbonates as a function of temperature, solution composition, and presence of a silicate mineral substrate. *Environ. Eng. Sci.* **2011**, *28*, 881−889.
(7) Ballirano, P.; De Vito, C.; Mignardi, S.; Ferrini, V. Phase transitions in the Mg-CO_2-H_2O system and the thermal decomposition of dypingite, $Mg_5(CO_3)_4(OH)_2{\cdot}5H_2O$: Implications for geosequestration of carbon dioxide. *Chem. Geol.* **2013**, *340*, 59−67.
(8) Botha, A.; Strydom, C. A. A. Preparation of magnesium hydroxy carbonate from magnesium hydroxide. *Hydrometallurgy* **2001**, *62*, 174−183.
(9) Lackner, K. S. Carbonate chemistry for sequestering fossil carbon. *Annu. Rev. Energy Environ.* **2002**, *27*, 193−232.
(10) Wilson, S. A.; Barker, S. L. L.; Dipple, G. M.; Atudorei, V. Isotopic disequilibrium during uptake of atmospheric CO_2 into mine process waters: Implications for CO_2 sequestration. *Environ. Sci. Technol.* **2010**, *44*, 9522−9529.
(11) Hövelmann, J.; Putnis, C. V.; Ruiz-Agudo, E.; Austrheim, H. Direct nanoscale observations of CO_2 sequestration during brucite [$Mg(OH)_2$] dissolution. *Environ. Sci. Technol.* **2012**, *46*, 5253−5260.
(12) Schaef, H. T.; Windisch, C. F.; McGrail, B. P.; Martin, P. F.; Rosso, K. M. Brucite [$Mg(OH_2)$] carbonation in wet supercritical CO_2: An in situ high pressure X-ray diffraction study. *Geochim. Cosmochim. Acta* **2011**, *75*, 7458−7471.
(13) Lackner, K. S.; Wendt, C. H.; Butt, D. P.; Joyce, E. L.; Sharp, D. H. Carbon dioxide disposal in carbonate minerals. *Energy* **1995**, *20*, 1153−1170.
(14) Nebel, H.; Neumann, M.; Mayer, C.; Epple, M. On the structure of amorphous calcium carbonate–a detailed study by solid-state NMR spectroscopy. *Inorg. Chem.* **2008**, *47*, 7874−7879.
(15) Papenguth, H. W.; Kirkpatrick, R. J.; Montez, B.; Sandberg, P. A. ^{13}C MAS NMR spectroscopy of inorganic and biogenic carbonates. *Am. Mineral.* **1989**, *74*, 1152−1158.
(16) Mason, H. E.; Kozlowski, A.; Phillips, B. L. Solid-state NMR study of the role of H and Na in AB-type carbonate hydroxylapatite. *Chem. Mater.* **2008**, *20*, 294−302.
(17) Sevelsted, T. F.; Herfort, D.; Skibsted, J. ^{13}C chemical shift anisotropies for carbonate ions in cement minerals and the use of ^{13}C, ^{27}Al and ^{29}Si MAS NMR in studies of Portland cement including limestone additions. *Cem. Concr. Res.* **2013**, *52*, 100−111.
(18) Hoyt, D. W.; Turcu, R. V. F.; Sears, J. A.; Rosso, K. M.; Burton, D.; Felmy, A. R.; Hu, J. Z.; Burton, S. D. High-pressure magic angle spinning nuclear magnetic resonance. *J. Magn. Reson.* **2011**, *212*, 378−385.
(19) Kwak, J. H.; Hu, J. Z.; Hoyt, D. W.; Sears, J. A.; Wang, C.; Rosso, K. M.; Felmy, A. R. Metal carbonation of forsterite in supercritical CO_2 and H_2O using solid state ^{29}Si, ^{13}C NMR spectroscopy. *J. Phys. Chem.C* **2010**, *114*, 4126−4134.
(20) Feng, J.; Lee, Y. J.; Reeder, R. J.; Phillips, B. L. Observation of bicarbonate in calcite by NMR spectroscopy. *Am. Mineral.* **2006**, *91*, 957−960.
(21) Bryce, D. L.; Bultz, E. B.; Aebi, D. Calcium-43 chemical shift tensors as probes of calcium binding environments. Insight into the structure of the vaterite $CaCO_3$ polymorph by ^{43}Ca solid-state NMR spectroscopy. *J. Am. Chem. Soc.* **2008**, *130*, 9282−9292.
(22) Pines, A.; Rhim, W. K.; Waugh, J. S. ^{13}C chemical shielding anisotropy in solids. CS_2 and $CaCO_3$. *J. Chem. Phys.* **1971**, *54*, 5438−5440.
(23) Lauterbur, P. Anisotropy of the C^{13} chemical shift in calcite. *Phys. Rev. Lett.* **1958**, *1*, 343−344.
(24) Sandengen, K.; Jøsang, L. O.; Kaasa, B. Simple method for synthesis of magnesite ($MgCO_3$). *Ind. Eng. Chem. Res.* **2008**, *47*, 1002−1004.
(25) Sayles, F. L.; Fyfe, W. S. The crystallization of magnesite from aqueous solution. *Geochim. Cosmochim. Acta* **1973**, *37*, 87−99.
(26) Felmy, A. R.; Qafoku, O.; Arey, B. W.; Hu, J. Z.; Hu, M.; Todd Schaef, H.; Ilton, E. S.; Hess, N. J.; Pearce, C. I.; Feng, J.; et al. Reaction of water-saturated supercritical CO_2 with forsterite: Evidence for magnesite formation at low temperatures. *Geochim. Cosmochim. Acta* **2012**, *91*, 271−282.
(27) Schaef, H. T.; McGrail, B. P.; Loring, J. L.; Bowden, M. E.; Arey, B. W.; Rosso, K. M. Forsterite [Mg_2SiO_4] carbonation in wet supercritical CO_2: An in situ high-pressure X-ray diffraction study. *Environ. Sci. Technol.* **2013**, *47*, 174−181.
(28) Davies, P. J.; Bubela, B. The transformation of nesquehonite into hydromagnesite. *Chem. Geol.* **1973**, *12*, 289−300.
(29) Surface, J. A. In situ high pressure and temperature ^{13}C NMR for the study of carbonation reactions of CO_2. Ph.D. Dissertation, Washington University in St. Louis, St. Louis, MO, 2013.
(30) Kloprogge, J. T.; Martens, W. N.; Nothdurft, L.; Duong, L. V.; Webb, G. E. Low temperature synthesis and characterization of nesquehonite. *J. Mater. Sci. Lett.* **2003**, *22*, 825−829.
(31) Massiot, D.; Fayon, F.; Capron, M.; King, I.; Le Calve, S.; Alonso, B.; Durand, J.-O.; Bujoli, B.; Gan, Z.; Hoatson, G. Modelling one- and two-dimensional solid-state NMR spectra. *Magn. Reson. Chem.* **2002**, *40*, 70−76.
(32) Giammar, D. E.; Bruant, R. G.; Peters, C. A. Forsterite dissolution and magnesite precipitation at conditions relevant for deep saline aquifer storage and sequestration of carbon dioxide. *Chem. Geol.* **2005**, *217*, 257−276.
(33) Xiong, W.; Giammar, D. Forsterite carbonation in zones with transport limited by diffusion. *Environ. Sci. Technol. Lett.* **2014**, *1*, 333−338.
(34) Akao, M.; Marumo, F.; Iwai, S. The crystal structure of hydromagnesite. *Acta Crystallogr., Sect. B: Struct. Crystallogr. Cryst. Chem.* **1974**, *30*, 2670−2672.
(35) Murdoch, J. Unit cell of hydromagnesite. *Am. Mineral.* **1954**, *39*, 24−29.
(36) Akao, M.; Iwai, S. The hydrogen bonding of hydromagnesite. *Acta Crystallogr., Sect. B: Struct. Crystallogr. Cryst. Chem.* **1977**, *33*, 1273−1275.
(37) Canterford, J. H.; Tsambourakis, G.; Lambert, B. Some observations on the properties of dypingite, $Mg_5(CO_3)_4(OH)_2{\cdot}5H_2O$, and related minerals. *Mineral. Mag.* **1984**, *48*, 437−442.
(38) Raade, G. Dypingite, a new hydrous basic carbonate of magnesium, from Norway. *Am. Mineral.* **1970**, *55*, 1457−1465.
(39) Yi, Y.; Liska, M.; Unluer, C.; Al-Tabbaa, A. Carbonating magnesia for soil stabilisation. *Can. Geotech. J.* **2013**, *50*, 899−905.
(40) Power, I. M.; Wilson, S. A.; Thom, J. M.; Dipple, G. M.; Southam, G. Biologically induced mineralization of dypingite by cyanobacteria from an alkaline wetland near Atlin, British Columbia, Canada. *Geochem. Trans.* **2007**, *8*.
(41) Hales, M. C.; Frost, R. L.; Martens, W. N. Thermo-raman spectroscopy of synthetic nesquehonite—Implication for the geo-sequestration of greenhouse gases. *J. Raman Spectrosc.* **2008**, *39*, 1141−1149.
(42) Dong, M.; Li, Z.; Mi, J.; Demopoulos, G. P. Solubility and stability of nesquehonite ($MgCO_3{\cdot}3H_2O$) in mixed NaCl + $MgCl_2$, NH_4Cl + $MgCl_2$, LiCl, and LiCl + $MgCl_2$ solutions. *J. Chem. Eng. Data* **2009**, *54*, 3002−3007.
(43) Stephan, G. W.; MacGillavry, C. H. The crystal structure of nesquehonite, $MgCO_3.3H_2O$. *Acta Crystallogr., Sect. B: Struct. Crystallogr. Cryst. Chem.* **1972**, *28*, 1031−1033.
(44) Ferrini, V.; De Vito, C.; Mignardi, S. Synthesis of nesquehonite by reaction of gaseous CO2 with Mg chloride solution: Its potential role in the sequestration of carbon dioxide. *J. Hazard. Mater.* **2009**, *168*, 832−837.
(45) Königsberger, E.; Königsberger, L.-C.; Gamsjäger, H. Low-temperature thermodynamic model for the system Na_2CO_3−$MgCO_3$−$CaCO_3$−H_2O. *Geochim. Cosmochim. Acta* **1999**, *63*, 3105−3119.
(46) Giester, G.; Lengauer, C. L.; Rieck, B. The crystal structure of nesquehonite, $MgCO_3{\cdot}3H_2O$, from Lavrion, Greece. *Mineral. Petrol.* **2000**, *70*, 153−163.

(47) Kwak, J. H.; Hu, J. Z.; Turcu, R. V. F.; Rosso, K. M.; Ilton, E. S.; Wang, C.; Sears, J. a.; Engelhard, M. H.; Felmy, A. R.; Hoyt, D. W. The role of H_2O in the carbonation of forsterite in supercritical CO_2. *Int. J. Greenhouse Gas Control* **2011**, *5*, 1081−1092.
(48) Fukushima, E.; Roeder, S. B. W. *Experimental Pulse NMR: A Nuts and Bolts Approach*; Addison-Wesley Publishing Company, 1981.